Solution Structure for *Pandinus* Toxin K-α (PiTX-Kα), a Selective Blocker of A-Type Potassium Channels[†,‡]

T. C. Tenenholz,[§] R. S. Rogowski,[||] J. H. Collins,[§,⊥] M. P. Blaustein,[||] and D. J. Weber*,[§]

*Departments of Biochemistry and Molecular Biology and of Physiology, University of Maryland School of Medicine,
and Department of Molecular Biology and Biophysics, Medical Biotechnology Center,
University of Maryland Biotechnology Institute, Baltimore, Maryland 21201*

ABSTRACT: PiTX-Kα, a 35-residue peptide recently isolated from the venom of *Pandinus imperator*, blocks the rapidly inactivating (A-type) K^+ channel(s) in rat brain synaptosomes and the cloned Kv1.2 potassium channel at very low toxin concentrations (6 nM and 32 pM, respectively) [Rogowski, R. S., Collins, J. H., O'Neil, T. J., Gustafson, T. A., Werkman, T. A., Rogawski, M. A., Tenenholz, T. C., Weber, D. J., & Blaustein, M. P. (1996) *Mol. Pharmacol. 50*, 1167−1177]. The three-dimensional structure of PiTX-Kα was determined using NMR spectroscopy in order to understand its selectivity and affinity toward K^+ channels. PiTX-Kα was found to have an α-helix from residues 10 to 21 and two β-strands (βI, 26−28; βII, 33−35) connected by a type II β-turn to form a small antiparallel β-sheet. Three disulfide bonds, which are conserved in all members of the charybdotoxin family (α-K toxins), anchor one face of the α-helix to the β-sheet. The N-terminal portion of PiTX-Kα has three fewer residues than other α-K toxins such as charybdotoxin. Rather than forming a third β-strand as found for other α-K toxins, the N-terminal region of PiTX-Kα adopts an extended conformation. This structural difference in PiTX-Kα together with differences in sequence at Pro-10, Tyr-14, and Asn-25 (versus Ser-10, Trp-14, and Arg-25 in CTX) may explain why PiTX-Kα does not block maxi-K^+ channels. Differences in three-dimensional structure between PiTX-Kα and charybdotoxin are also observed in both the tight turn and the loop that connects the first β-strand to the α-helix. As a result, side chains of two residues (Tyr-23 and Arg-31) are in regions of PiTX-Kα that probably interact with rapidly inactivating A-type K^+ channels. The analogous residues in charybdotoxin are positioned differently on the toxin surface. Thus, the locations of Tyr-23 and Arg-31 side chains in PiTX-Kα could explain why this toxin blocks A-type channels at much lower concentrations than does charybdotoxin.

Pandinus toxin K-α is a newly identified (Rogowski *et al.*, 1996) member of the α-K toxin family of proteins (Miller, 1995). This group of small peptides (∼4 kDa), derived from the venoms of both new and old world scorpions, selectively blocks certain subtypes of voltage-gated and Ca^{2+}-dependent K^+ channels (Miller, 1995). Unlike most other α-K toxins, *Pandinus* toxin K-α (PiTX-Kα)[1] preferentially blocks rapidly inactivating, voltage-gated K^+ channels with high potency ($IC_{50} = 6$ nM). It is also the most potent inhibitor ($IC_{50} = 32$ pM) of Kv1.2 channels yet identified (Rogowski *et al.*, 1996). The three-dimensional structures for several members of the α-K toxin family have been determined by NMR spectroscopy; they all show nearly identical patterns of secondary structure and very similar global folds (Bontemps *et al.,* 1992; Johnson & Sugg, 1992; Johnson *et al.,* 1994; Aiyar *et al.,* 1995; Krezel *et al.,* 1995; Miller, 1995). The three disulfide bonds and several positively charged residues are conserved in PiTX-Kα, but the precise determinants of its selectivity and affinity are unknown.

A preliminary model for the binding of PiTX-Kα to the K^+ channel vestibule was proposed in order to explain its selectivity and high affinity for A-type channels (Rogowski *et al.,* 1996).[2] In this model, PiTX-Kα binds to the channel with residue Lys-27 blocking the K^+-selective ion conduction

---

Table 1: Sequence Alignment of Three *Pandinus* Toxins (Rogowski *et al.*, 1996) with Selected Toxins from Other α-KTX Subfamilies[a]

Toxin	Sequence
	5······10·····15····20····25·····30····35
CTX	Z F T N V S C T T S K E - C W S V C Q R L H N T S R - G K C M N K K C R C Y S
PiTX -Kα	T I S C T N P K Q - C Y P H C K K E T G Y P N - A K C M N R K C K C F G R
PiTX -Kβ	T I S C T N E K Q - C Y P H C K K E T G Y P N - A K C M N R K C K C F G R
PiTX -Kγ	L V K C R G T S D - C G R P C Q Q Q T G C P N - S K C I N R M C K C Y G C
MgTX	T I I N V K C T - S P K Q C L P P C K A Q F G Q S A G A K C M N G K C K C Y P
KTX	V E I N V K C S G S P - Q C L K P C K D A - G M R F G - K C M N R K C H C T P ?
AgTX2	V P I N V S C S G S P Q - C I K P C K D A - G M R F - G K C M N R K C H C T P K

[a] Residue numbering is that of CTX, in order to facilitate comparisons to other toxins. For CTX, residues which are critical (closed symbols) or influential (open symbols) for binding to single Ca^{2+}-dependent (●, ○) (Stampe *et al.*, 1994) or cloned Shaker F425G (■, □) (Goldstein *et al.*, 1994) K^+ channels are indicated. Representative toxins from previously defined subfamilies (Miller, 1995) include margatoxin (MgTX; Garcia-Calvo *et al.*, 1993), kaliotoxin (KTX; Crest *et al.*, 1992), and agitoxin (AgTX2; Krezel *et al.*, 1995). The amino-terminal glycines of KTX and AgTX2 are omitted.

pore (Rogowski *et al.*, 1996), as is the case for CTX (Park & Miller, 1992a,b; Anderson *et al.*, 1988; Miller, 1988, 1990; Goldstein *et al.*, 1994; Stampe *et al.*, 1994; MacKinnon & Miller, 1988).[3] The residues surrounding Lys-27 are believed to modulate the affinity and specificity of the toxin for different K^+ channel subtypes (Table 1; Rogowski *et al.*, 1996; Miller, 1995; Stampe *et al.*, 1994; Goldstein *et al.*, 1994).

The three-dimensional structure of PiTX-Kα used in the aforementioned model was calculated using an energy minimization protocol, and it was assumed that PiTX-Kα has the same fold as a very well characterized α-K toxin, CTX (Rogowski *et al.*, 1996). While useful, this preliminary model was based on several assumptions about the structure of PiTX-Kα. First, the three proline residues in PiTX-Kα were all assumed to be in the *trans* configuration. This assumption requires verification by NMR spectroscopy since related toxins are known to contain *cis* prolines (Lebreton *et al.*, 1994). Additionally, the sequence of PiTX-Kα has three fewer residues at the N-terminus when compared to CTX. Since the first three residues of CTX participate in an antiparallel β-sheet, the absence of these residues in PiTX-Kα could have unpredictable effects. Therefore, we pro-

[2] In this article, A-type refers to the channel type(s) responsible for both the current observed in *Xenopus* oocytes expressing a Shaker (Δ6−46; F425G) K^+ channel (Goldstein & Miller, 1992, 1993) and the voltage-gated, rapidly inactivating Rb^+ flux observed in synaptosomes (Schneider *et al.*, 1989). Similarly, maxi-K^+ refers to the channel type-(s) responsible for both the current observed in lipid bilayers containing a large-conductance Ca^{2+}-dependent K^+ channel from rat skeletal muscle (Anderson *et al.*, 1988) and the Ca^{2+}-dependent component of Rb^+ efflux observed in rat brain synaptosomes (Schneider *et al.*, 1989).

[3] Due to the presence of three additional residues at the N-terminus of CTX which are not present in PiTX-Kα isolated from *Pandinus imperator*, the sequence alignment is shifted by three residues. It is necessary to adopt a uniform numbering system to make comparisons between these two toxins. A numbering system based on the sequence of CTX was chosen to facilitate comparison to the existing literature. We therefore assign the N-terminal Thr of PiTX-Kα the sequence number 4, despite the fact that it is the first residue in the sequence of the natural toxin. Consecutive numbering of the remaining residues in PiTX-Kα keeps the alignment in frame with that of CTX.

duced milligram quantities of fully active recombinant PiTX-Kα and determined its structure in solution using two-dimensional NMR spectroscopy. Interestingly, an analysis of the NMR structure of PiTX-Kα revealed several structural differences between it and CTX. These differences enabled us to clarify how PiTX-Kα selectively binds A-type K^+ channels with a higher affinity than CTX. Furthermore, a structural basis is discussed for why, in contrast to CTX, PiTX-Kα does not block Ca^{2+}-dependent large conductance (maxi) K^+ channels. A preliminary abstract of this work has been published (Tenenholz *et al.*, 1996).

EXPERIMENTAL PROCEDURES

NMR Sample Preparations. Expression and purification of recombinant PiTX-Kα were performed on a large scale using procedures similar to those described previously for a smaller scale preparation (Rogowski *et al.*, 1996). The overexpression plasmid contains a synthetic gene coding for PiTX-Kα inserted into the pSR9 expression plasmid under the control of a T7 promoter (Howell & Blumenthal, 1989). In this construct, the toxin is part of a 40 kDa fusion protein containing T7 gene 9 sequences, the pFLAG epitope (Park *et al.*, 1989), and an enterokinase site linked to the toxin sequence (Rogowski *et al.*, 1996). Typically, *Escherichia coli* BL21(DE3) cells transfected with the expression plasmid were grown in 8−10 L of LB at 37 °C (Maniatis *et al.*, 1989) and induced with IPTG (0.5 mM). Following sonication and lysozyme treatment (in 10 mM Tris buffer, pH 8, containing 50 mM NaCl, 2 mM EDTA, 2 mg/mL lysozyme, 0.14 mg/mL PMSF, 0.2 μg/mL leupeptin, 0.2 μg/mL pepstatin, and 0.04% β-mercaptoethanol), soluble fusion protein was found to be the major band in a SDS−PAGE gel of the cell lysates. DNA was removed by centrifugation after the slow addition of streptomycin sulfate at 4 °C to a final concentration of 3%. The fusion protein was then precipitated by the slow addition of solid ammonium sulfate at 4 °C to a final concentration of 50%, dialyzed, and separated from other cellular proteins using a DEAE-cellulose (DE52) anion-exchange column (Whatman Inc., Maidstone, England) with a linear salt gradient of 50−500 mM NaCl. Dialysis into a low salt buffer (10 mM Tris, 1 mM β-mercaptoethanol, pH 8.0) preceded treatment of the fusion protein (24 h at 37 °C) with fresh enterokinase (Biozyme Inc., San Diego, CA, 200 units of enzyme/mg of fusion protein) in 5 mM $CaCl_2$ in order to cleave the toxin from the fusion protein. HPLC separation on an Aquapore CX-300 cation-exchange column (Pierce, Rockford, IL) was followed by reverse-phase chromatography on an Aquapore RP-300/C18 column (Pierce, Rockford, IL) to yield pure PiTX-Kα (>99%). HPLC solvents and trace amounts of metals were removed prior to NMR spectroscopy using two rounds of dialysis in 500 MW cutoff membranes (Spectrapor, Los Angeles, CA) with deuterated Tris (0.25 mM Tris-d_{11}, pH 7.4) and 0.03% Chelex-100 (Bio-Rad, Hercules, CA) in the dialysate buffer. Protein sequencing of the entire peptide confirmed that the sequence was identical to the naturally occurring toxin. A ^{86}Rb efflux assay (Blaustein *et al.*, 1991) confirmed that the channel blocking activity and specificity of the recombinant toxin were identical to those of PiTX-Kα isolated directly from scorpion venom (Rogowski *et al.*, 1996).

Samples for the TOCSY and ROESY experiments were prepared by dissolving 3.8 mg of the lyophilized toxin (1.8 mM) in a buffer containing 1.9 mM Tris-d_{11}, 0.34 mM NaN_3,

0.1 mM EDTA, and 10% D_2O to a final volume of 525 μL. Minute amounts of cold NaOH and HCl were added to adjust the pH to 3.45. A higher concentration NMR sample was prepared in a small sample volume tube (Shigemi Inc., Allison Park, PA) for DQF-COSY and NOESY spectra. This sample contained 3.7 mM toxin, 0.7 mM NaN_3, 0.2 mM EDTA, 10% D_2O, and 3.9 mM Tris-d_{11}, pH 3.45, in a final volume of 255 μL. The higher concentration sample was also used to collect data in 100% D_2O with an uncorrected pH value of $\approx$3.0. [86]Rb efflux assays (Blaustein *et al.*, 1991) repeated at the end of the NMR data collection period indicated that the toxin retained all (>99%) of its biological activity.

NMR Experiments. Proton NMR data used in the structure calculations were collected at 600.13 MHz using a Bruker DMX-600 spectrometer (Bruker Inc., Billerica, MA). Spectra were acquired with a sweep width in both proton dimensions of 7184 Hz. A typical experiment acquired 2K t_2 and 512 or 1024 t_1 data points, respectively. Solvent suppression was achieved using the WATERGATE sequence (Piotto *et al.*, 1992) or by selective saturation of the H_2O and HDO resonances during the initial delay. All experiments were conducted at 37 °C and were referenced to the residual water signal (4.658 ppm) as a secondary reference to TSP, 3-(trimethysilyl)[2,2,3,3-²H₄]propionate. Data were processed off-line using FELIX (Molecular Simulations, San Diego, CA) on a Silicon Graphics Indy workstation (Silicon Graphics Inc., Mountain View, CA). Data were multiplied by a sine-squared bell and zero-filled to 2048 points in both dimensions prior to Fourier transformation.

Spin system identification and sequence-specific assignments were determined as previously described (Wüthrich, 1986) using a 2D DQF-COSY (Piantini *et al.,* 1982; Rance *et al.,* 1983), a 2D TOCSY collected with a 70 ms spin-lock time (Bax & Davis, 1985; Griesinger *et al.,* 1988), and several 2D NOESY (Macura & Ernst, 1980) experiments collected with 50, 150, and 200 ms mixing times. Additionally, a ROESY spectrum (Griesinger & Ernst, 1987) was collected with a 100 ms spin-lock mixing time, and the resulting data were used to correct NOESY data for spin diffusion effects. A PE-COSY was collected in D_2O in order to obtain passive and active $^3J_{H\alpha-H\beta}$ coupling constants as previously described (Griesinger *et al.,* 1985, 1987).

Hydrogen exchange rates were observed by lyophilizing PiTX-Kα from H_2O and redissolving it in 99.96% D_2O (Aldrich, Milwaukee, WI). A series of 2D DQF-COSY spectra were initiated at 5, 25, 70, and 150 min after the addition of D_2O. Similarly, in a separate experiment, a series of 1D experiments (128 scans of 16 384 data points) were acquired every 3 min after the addition of D_2O for $\approx$3 h as previously described for other low molecular weight toxins (Lebreton *et al.,* 1994).

Structure Calculations. Spin system identification and assignment were achieved by comparison and analysis of the DQF-COSY, TOCSY, and NOESY experiments as previously described (Wüthrich, 1986). Analysis of NOESY and ROESY spectra was used to assign 295 ¹H—¹H NOE correlations which were divided into strong (1.8−2.8 Å), medium (1.8−3.3 Å), weak (1.8−5.0 Å), and very weak (1.8−6.0 Å) categories. Internal calibration of cross-peak intensities was achieved by comparing several $d_{\alpha N}(i,i + 3)$ correlations observed for PiTX-Kα, which have a known distance of $\approx$3.4 Å in α-helices, to other correlations in the

same NOESY or ROESY spectrum. Rotational conformations about χ were determined using a combination of $^3J_{H\alpha-H\beta}$ coupling constants and NOE information about H_α/H_β and H_N/H_β (Basus, 1989) and were assigned to trans, gauche-(+), or gauche(−) rotamers with a tolerance of $\pm$40°. Stereospecific assignment of eight methylene protons, as well as the lone isoleucine side chain, resulted in nine χ dihedral angle restraints. Nine hydrogen bond constraints were derived from amide exchange data and NOE cross-peaks characteristic of α-helix and β-sheet secondary structural elements. These H_N−O distances were assigned a lower limit of 1.5 Å and an upper limit of 2.3 Å. The three disulfide bridges were replaced by distance constraints (2.0−2.03 Å) between the S_γ atoms during the matrix sub-embedding step. Structures calculated without these hydrogen and disulfide bond restraints showed no significant changes (backbone rmsd <0.8 Å).

Structural calculations were performed using the program X-PLOR 3.1 (Brünger, 1992) with a standard distance geometry−simulated annealing protocol (Nilges *et al.,* 1988). In this procedure, a random set of template coordinates generated by X-PLOR resulted in models for PiTX-Kα with extended conformations. Following distance matrix generation and substructure embedding, each structure was then subjected to simulated annealing using 3 ps of high temperature (2000 K) dynamics and 5 ps of cooling to 100 K. Structure refinement used 10 ps of slow cooling from 1000 to 100 K in 50 K steps followed by 200 steps of Powell minimization. NOE constraints used a center-averaged, square well potential with a K_{NOE} of 50 kcal mol⁻¹ Å⁻¹ and an exponent of 2, and this potential was held constant throughout simulated annealing and refinement procedures. Beginning with only the unambiguously assigned NOE correlations, several preliminary structures were calculated. These structures were used to assign additional NOE correlations. Subsequently, a NOE back-calculation protocol in X-PLOR was used to refine the NOE-derived distance restraints, as similarly described for other low molecular weight toxins (Brünger, 1992; Lebreton *et al.,* 1994). A total of 194 interresidue, 101 intraresidue, and 9 hydrogen-bonding distance constraints, as well as 9 dihedral angle (χ) constraints, were used to calculate 500 structures for PiTX-Kα. Twenty unique structures were identified as being acceptable since they had no distance violations greater than 0.30 Å, no angular violations greater than 5°, and a total energy less than 120 kcal mol⁻¹. All 20 structures had no residues outside the allowed regions of a Ramachandran plot.

RESULTS

Sequential Proton Assignments. Assignment of NMR signals for PiTX-Kα was performed according to standard protocols (Wüthrich, 1986). Coupled spin networks were identified using data from TOCSY and DQF-COSY spectra in both H_2O and D_2O. Following identification of H_α−H_N cross-peaks in the DQF-COSY, spin systems for all but the amino-terminal amide proton (Thr-4)[3] were identified using relayed TOCSY connectivities in H_2O. The assignment of spin systems was confirmed in upfield regions of TOCSY spectra in H_2O and D_2O for cases where dispersion was adequate. Aromatic ring protons were assigned using TOCSY correlations in the aromatic region and distinguished by NOE correlations observed between ring and H_β and H_α

protons in NOESY spectra collected in D$_2$O (Wüthrich, 1986).

Sequence-specific assignments for protons of PiTX-Kα were made using interresidue connectivities (αN, NN, βN, etc.) determined from the 2D NOESY experiment (Wüthrich, 1986). In all cases, NOESY and ROESY data were compared in order to distinguish chemical exchange correlations from NOE correlations and to determine contributions to signal intensity from spin diffusion effects in the NOESY experiment. Starting positions for tracing sequential connectivities included the unique isoleucine residue at position 5, the glycine residue at position 22, the alanine residue at position 26, and the unique Gly-Arg pair at positions 37 and 38, respectively. Strong $d_{\alpha N}(i,i + 1)$ NOE correlations were used primarily to establish the connectivity of spin systems for residues 5−8 and 24−38, whereas strong $d_{NN}(i,i + 1)$ NOE cross-peaks were used to identify sequence-specific assignments for residues 8−9, 11−14, and 16−23. A gap in the $d_{NN}(i,i + 1)$ connectivities at position 15 was expected due to the presence of a proline residue, but a sequential connectivity [$d_{\delta N}(i,i + 1)$] confirmed the location of this residue. Furthermore, strong H$_\delta$−H$_\alpha$ ($i,i − 1$) or H$_\delta$−H$_N$($i,i − 1$) NOE cross-peaks were observed between residues 10 and 9, residues 15 and 14, and residues 24 and 23. This established that all of the proline residues are in the *trans* configuration and confirmed their positions in the sequence. Observation of an NOE correlation between the β-proton of residue 4 (whose amide proton was not detected) and the amide proton of residue 5 completed the sequential assignment for PiTX-Kα (see spectra and table in Supporting Information).

Secondary Structure. NOE correlations and chemical shift values were used to identify elements of secondary structure in PiTX-Kα (Figure 1; Wüthrich, 1986; Wishart *et al.,* 1992). The presence of strong H$_N$−H$_N$ NOE correlations from residues 11 to 21 (except at Pro-15) and the finding that the chemical shift values of the α-protons of residues 10−21 are generally negative with respect to random coil values (Wishart *et al.,* 1992) together indicate a helical conformation for this segment. The $d_{\alpha N}(i,i + 3)$ interaction from Pro-10 to Cys-13, combined with the negative chemical shift index of Pro-10, establishes Pro-10 as the initial residue of the α-helix, while the presence of d$_{\alpha N}(i,i + 3)$ and ($i,i + 4$) interactions involving the amide proton of Thr-21 are evidence that it is the last residue of the helix. The presence of a helix from residues 10 to 21 is confirmed by the presence of six $d_{\alpha N}(i,i + 3)$ connectivities, two of which (C13-H16 and Y14-C17) span the potentially helix-breaking Pro-15 residue. Furthermore, two $d_{\alpha N}(i,i + 4)$ NOE correlations (H16-E20 and C17-T21) clearly identify residues 16−21 as being α-helical (Figure 1). While other studies of α-K toxins (Krezel *et al.,* 1995) report the presence of 3$_{10}$ helix character for the N-terminal portion of the helix, the presence of d$_{\alpha N}$-($i,i + 4$) and the absence of d$_{\alpha N}(i,i + 2)$ NOE correlations rule out this possibility for PiTX-Kα.

Strong $d_{\alpha N}$ connectivities from residues 26 to 28 and 33 to 35 together with a positive chemical shift index for the α-protons in these segments indicate β-strand conformation. Furthermore, seven long-range (i,j) NOE interactions ($d_{\alpha N}$-[26:36, 28:34, 35:27, 33:29]; d_{NN}[27:34]; $d_{\alpha\alpha}$[26:35, 28:33]) establish that these two β-strands align to form a small two-stranded antiparallel β-sheet (Figure 2). The two β-strands are separated by residues 29−32, which have $d_{\alpha N}$ and d_{NN}
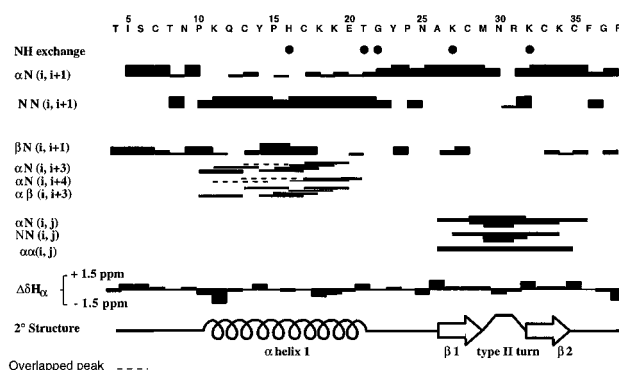

FIGURE 1: Amino acid sequence of PiTX-Kα and summary of NOE connectivities used for sequential assignment and secondary structure determination. Data are summarized from NOESY and ROESY spectra collected at 310 K, pH 3.45, in 90%/10% H$_2$O/D$_2$O, using a mixing time of 200 ms. Overlapping NOE correlations are illustrated with dashed lines and rectangles. Slowly exchanging amide protons are indicated by dark circles. For proline residues, sequential NOE correlations involving H$_\delta$ rather than H$_N$ are shown. The chemical shift deviations for each α-proton (Δδ H$_\alpha$) are indicated by an upward or downward pointing rectangle. The size of the rectangle represents the magnitude of deviation from the random coil value, and no rectangle indicates a shift index of zero (Wishart *et al.,* 1992). Secondary structure elements determined from all of the data are also shown.
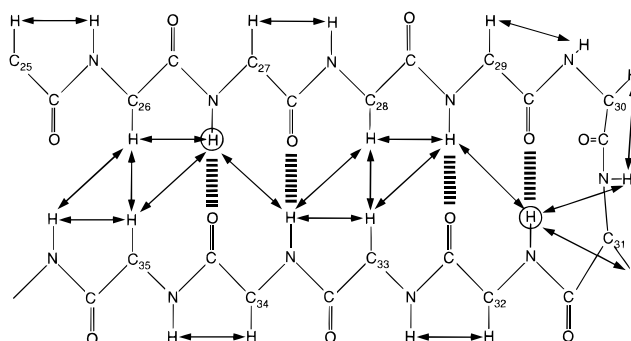

FIGURE 2: Schematic diagram for the β-sheet region of PiTX-Kα. Observed NOE cross-peaks are indicated by double-headed arrows. Slowly exchanging amide protons are circled, and hydrogen bonds used in the structural calculations are shown as dashed lines.

NOE correlations expected of a tight turn (Wüthrich, 1986). Although the $d_{\alpha N}$ NOE correlation between residues 30 and 31 (which is typical of a type II turn) overlaps with another resonance in the protein, the presence of a d_{NN} NOE correlation between residues 31 and 32 was assigned unambiguously. Type I and I′ turns were ruled out because the d_{NN} NOE correlation observed between residues 30 and 31 in the NOESY spectrum was absent in the 2D ROESY experiment, indicating that spin diffusion was the major contributor to this cross-peak (data not shown).

All of the previously studied members of the α-K toxin family contain a three-stranded antiparallel β-sheet with one strand of the β-sheet coming from the N-terminal region of the toxin (Miller, 1995). In PiTX-Kα, however, three residues at the N-terminus are absent when the amino acid sequence of PiTX-Kα is compared to other α-K toxins [Table 1 and see Rogowski *et al.* (1996)], and no NOE correlations characteristic of a third β-strand in the antiparallel β-sheet were observed for PiTX-Kα. In fact, the first residue of PiTX-Kα is relatively unstructured, with few NOE correlations, and a chemical exchange cross-peak for the α-proton of Thr-4 is observed in the ROESY spectrum (not shown). This exchange cross-peak indicates that two alternative

FIGURE 3: NMR structure of PiTX-Kα. (A) Stereo overlay of the 20 best structures determined as described in Experimental Procedures. Selected side chains are shown in magenta. The backbone RMSD for these 20 structures is 1.16 Å. (B) Ribbon diagram for PiTX-Kα illustrating the single α-helix, two-stranded antiparallel β-sheet, and disulfide bonding.

conformations for the N-terminus exist in solution. Thus, PiTX-Kα forms a two-stranded β-sheet, with the C-terminal strand (strand II) corresponding to the central strand found in CTX (Figures 1 and 2).

Tertiary Structure. The structure of PiTX-Kα was calculated using 295 NOE distance constraints (8.4 per residue) and 9 χ dihedral angle restraints (Figure 3). The 20 accepted structures for PiTX-Kα shown in Figure 3 illustrate that all of the calculated structures have the same overall backbone fold. The average pairwise RMSD for these structures is 1.16 Å for backbone atoms and 2.09 Å for all heavy atoms, and if the poorly determined N- and C-terminal residues are excluded from the calculation, the RMSD values are 0.802 and 1.57 Å, respectively (Table 2). When an average structure was calculated from the 20 selected structures, the RMSD to this mean structure was found to be 0.818 Å for the backbone atoms and 1.46 Å for all heavy atoms (Table 2). The Ramachandran diagram of the best-fit structure (Supporting Information) shows that all residues of this toxin are either in the most favored region (74%) or in the additionally allowed regions (26%).

Disulfide Bonds. Conservation of the disulfide bridging pattern found in other α-K toxins was expected for PiTX-Kα. Strong $H_\beta-H_\beta$ interactions between residues 13:33 and 17:35 confirmed these disulfides, and the NOE correlations between residues 7:28 were less well resolved, but still present. These disulfide bonds establish the orientation of the α-helix relative to the β-sheet, by anchoring one face of the helix (residues 13 and 17) to strand II of the β-sheet (residues 33 and 35) and the N-terminal region of the toxin (residue 7) to strand I (residue 28). The disulfides occupy the cores of other α-K toxins, and the presence of multiple long-range NOE cross-peaks to the methylene protons of the cysteine residues demonstrates that they are similarly located in PiTX-Kα. In addition, long-range NOE cross-peaks to the side chains of Ile-5 (6 correlations), His-16 (10 correlations), and Ala-26 (8 correlations) provide evidence that these residues are also in the core of the protein. Finally, calculations of the structure without disulfide bonds did not affect the tertiary structure, indicating that the pairing of cysteine residues to form disulfide bonds is correct.

Structural Similarities to Other α-K Toxins. The overall structure of PiTX-Kα is similar, in many respects, to those of other members of the α-KTX family including CTX (Bontemps *et al.,* 1992), IbTX (Johnson & Sugg, 1992), MgTX (Johnson *et al.,* 1994), KTX (Aiyar *et al.,* 1995), and AgTX2 (Krezel *et al.,* 1995). All of these toxins contain a single α-helix connected to an antiparallel β-sheet by a small loop. While the antiparallel β-sheet of PiTX-Kα differs from that of other α-K toxins (such as CTX) in that it contains only two β-strands rather than three, the orientation of this

Table 2: NMR-Derived Restraints and Statistics of NMR Structures

structural statistic	⟨20⟩	best
RMSDs (Å)		
all restraints (312)	0.024 ±0.002	0.022
intraresidue (101)	0.023 ±0.003	0.022
sequential (90)	0.035 ±0.003	0.033
medium range (43)	0.004 ± 0.002	0.002
long range (60)	0.005 ± 0.003	0.007
hydrogen bond (18)	0.020 ± 0.003	0.018
max dist viol (Å)	0.220 ± 0.009	0.224
RMSD dihedral (deg)	0.168 ± 0.150	0.221
max dihed viol (deg)	0.670 ± 0.009	0.662
RMSDs (covalent geom)		
bonds (Å)	0.003 ± 0.000	0.002
angles (deg)	0.702 ± 0.006	0.695
impropers (deg)	0.474 ± 0.012	0.454
X-PLOR energies (kcal/mol)		
total	101.36 ± 3.20	96.49
bonds	3.75 ± 0.26	3.46
angles	76.27 ± 1.22	74.66
repel	2.53 ± 0.86	1.81
NOE	8.26 ± 1.15	7.47
cdih	0.028 ± 0.036	0.027
Lennard-Jones energy	−71.44 ± 8.73	−90.33

RMSDs for ⟨20⟩ (Å)	relative to mean	pairwise
backbone (5–37)	0.554	0.80 ± 0.14
heavy atoms (5–37)	1.086	1.57 ± 0.17
backbone (all)	0.818	1.16 ± 0.30
heavy atoms (all)	1.460	2.09 ± 0.41

RMSDs to CTX (Å)	relative to best structure
secondary structure (11–21, 26–28, 33–35)	0.93
backbone (5–36)	1.28
heavy atoms (5–36)	4.29
backbone (all)	1.58
heavy atoms (all)	3.85

[a] ⟨20⟩ indicates the ensemble of 20 low-energy structures meeting the criteria described in Experimental Procedures, and "best" indicates the lowest energy member of the ensemble. For the ensemble of 20 low-energy structures, values are given as mean ± standard deviation. The Lennard-Jones van der Waals energy was calculated using the CHARMM19 parameters and was not employed in any stage of the structure determination.

smaller β-sheet with respect to the α-helix is preserved; the α-helix and N-terminal portions of all the α-K toxins interact with the same face of the smaller β-sheet. This is reflected in the backbone RMSD between PiTX-Kα and corresponding residues of CTX (residues 4–37). When all residues are included, this RMSD is 1.58 Å, but when only residues involved in the α-helix and the two β-strands are considered, the RMSD is reduced to 0.93 Å (Table 2).

Structural Differences from Other α-K Toxins. A difference is observed for PiTX-Kα, however, when its amino acid sequence is compared to CTX and the consensus

sequence (G_{26}-[*]-K_{27}-C_{28}-$(M/I)_{29}$-$(N/G)_{30}$-X_{31}-K_{32}-C_{33}-$(\pm)_{34}$-C_{35}) for α-K toxins (Miller, 1995). PiTX-Kα contains an alanine residue at position 26 rather than a glycine residue as for other α-K toxins (Bontemps, 1991; Miller, 1995). The positioning of Ala-26 in the core of the protein is unambiguous since eight long-range NOE interactions between the methyl protons of this residue and residues on both sides of the molecule (C35, F36, K27, Y14, C13, C17, and C33) allow for no other possibility. Despite the presence of an alanine at this position, the structure of the toxin in the region of Ala-26 does not significantly vary from that observed for CTX. In addition, PiTX-Kα lacks three residues at the N-terminus when compared to other α-K toxins. Since there are at least two other toxins derived from *Pandinus imperator* (PiTX-Kβ and PiTX-Kγ), which have similar sequences (Rogowski *et al.,* 1996), we propose a new subfamily of α-K toxins. Under the formal nomenclature (Miller, 1995) this subfamily is designated α-KTX5.*x*. When the conserved cysteine residues of these toxins are aligned with CTX (α-KTX1.1), the members of this subfamily all contain an N-terminal region which is three residues shorter than other α-K toxins, and all have a relaxed consensus sequence allowing an alanine and perhaps a serine residue (rather than glycine exclusively) at position 26.

Comparison to the Computer-Generated Homology Model. The structure of PiTX-Kα determined here by NMR confirms the global fold of a computer-generated model for the structure of PiTX-Kα determined previously (Rogowski *et al.,* 1996). This model was calculated using an energy minimization protocol based on amino acid sequence homologies of α-K toxins and presumed structural similarities to CTX. However, comparison of this model to the NMR structure reveals differences at the N-terminus of the toxin. These differences probably arise because CTX, which contains a third β-strand, was used as the starting structure for the modeling protocol. Other differences are also observed in the C-terminus and the loop which connects the α-helix to the first β-strand. The homology model also does not agree with several side chain orientations that are well determined in solution by NMR-derived constraints. This latter point is important because the locations of side chain residues are critical for analyzing the interactions between α-K toxins and K$^+$ channels (Goldstein *et al.,* 1994; Hidalgo & MacKinnon, 1995; Stampe *et al.,* 1994; Aiyar *et al.,* 1995).

DISCUSSION

The goal of this study was to determine the three-dimensional structure of PiTX-Kα by NMR spectroscopy in order to elucidate the features responsible for its selectivity and affinity toward K$^+$ channels. The structure of PiTX-Kα was found to have a tertiary fold similar to that of CTX. The amino acid residue (K27) that inserts into the channel pore and is critical for the voltage sensitivity of CTX channel-blocking activity (Park & Miller, 1992b; Bontemps *et al.,* 1991) is located in the same position in PiTX-Kα (Figure 4; Rogowski *et al.*, 1996). Furthermore, several other residues in PiTX-Kα (M29, N30, K34), which surround this lysine residue (K27), are also located in similar positions to analogous residues in CTX (Figure 4A). The side chains from these four conserved residues are most likely involved in critical interactions between PiTX-Kα and the channel vestibule (Table 1), as previously found for CTX and other α-K toxins (Goldstein *et al.,* 1994; Stampe *et al.,* 1994).
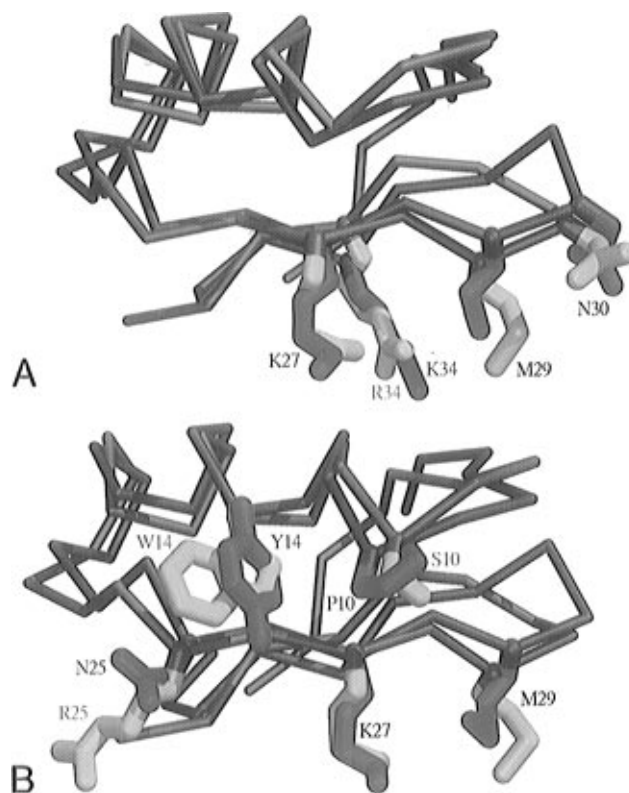

FIGURE 4: Comparison of structures for CTX (Bontemps *et al.,* 1992) and PiTX-Kα. Overlay of α-carbon traces (gray, tinted with yellow for CTX or magenta for PiTX-Kα). Selected side chains are shown for both CTX (yellow) and PiTX-Kα (magenta). (A) Highly conserved residues (M29, N30, K34) surrounding K27, which occludes the ion conduction pore. (B) Side chains critical for interaction with maxi-K channels. Conserved residues (K27, M29) are labeled in black, while the nonconserved residues governing selectivity for (yellow) or against (magenta) maxi-K$^+$ channels are labeled for both toxins.

There are many obvious structural similarities between PiTX-Kα and CTX. Nevertheless, the functional properties of these two toxins are clearly quite different. In rat brain synaptosomes, CTX blocks both maxi-K$^+$ ($IC_{50} = 15$ nM) and Ca^{2+}-independent rapidly inactivating (A-type) K$^+$ channels ($IC_{50} = 40$ nM) (Blaustein *et al.,* 1991). These two types of channels in rat brain appear to be analogous to the maxi-K$^+$ channel ($K_D = 8.8$ nM; Stampe *et al.,* 1994) and the cloned Ca^{2+}-independent Shaker channel, respectively ($K_D = 148$ nM; Goldstein & Miller, 1992). In contrast to CTX, PiTX-Kα potently and specifically blocks only the A-type channel in rat brain synaptosomes and does so with higher affinity ($IC_{50} = 6$ nM versus 40 nM for CTX; Blaustein *et al.,* 1991). In the same preparation, 500 nM PiTX-Kα does not block maxi-K$^+$ channels. Additionally, PiTX-Kα has an exceptionally high affinity ($IC_{50} = 32$ pM) for Ca^{2+}-independent cloned Kv1.2 channels (Rogowski *et al.,* 1996), whereas CTX binds to this channel with lower affinity ($K_D \approx 2-14$ nM; Grissner *et al.,* 1994; Werkman *et al.,* 1992). Accordingly, a detailed analysis of subtle differences in side chain type and positioning between PiTX-Kα and other α-K toxins (such as CTX) is needed to explain why PiTX-Kα blocks A-type but not maxi-K$^+$ channels.

Why PiTX-Kα Does Not Block Maxi-K$^+$ Channels. The residues at positions 10, 14, 25, and 29 are particularly interesting because mutations at these positions in CTX (S10, W14, R25, and M29) have larger effects on binding to maxi-K$^+$ channels (Stampe *et al.,* 1994) than to A-type channels

(Table 1; Goldstein *et al.*, 1994). For example, mutation of Ser-10 in CTX to glutamine decreases the affinity for the maxi-K$^+$ channel 1500-fold (Stampe *et al.,* 1994), whereas the same mutation produces only an 18-fold decrease in affinity for the A-type Shaker F425G channel (Goldstein *et al.,* 1994). Likewise, mutations of Trp-14 (W14A, W14M, W14Y, W14F, W14Q), Arg-25 (R25Q), and Met-29 (M29I, M29L) in CTX dramatically decrease the toxin's affinity for maxi-K$^+$ channels but have smaller effects on CTX binding to A-type Shaker K$^+$ channels (Stampe *et al.,* 1994; Goldstein *et al.,* 1994). Furthermore, all four of these residues are conserved in other α-K toxins that block maxi-K$^+$ channels (e.g., CTX, Lq2, LbTX, and IbTX; Miller, 1995).

Interestingly, the analogous residues in PiTX-Kα (P10, Y14, N25, and M29) form a surface that partially encircles Lys-27 (Figure 4). Furthermore, the backbone structure in this region is similar to that of CTX, despite the presence of a proline residue (P10) in the α-helix of PiTX-Kα (Figure 4B). However, three of the four residues that are necessary for binding maxi-K$^+$ channels in CTX (S10, W14, R25) are different in PiTX-Kα (P10, Y14, N25). It is therefore not surprising that maxi-K$^+$ channels in rat brain synaptosomes are not inhibited by PiTX-Kα. Thus, the chemical properties of side chain moieties at positions P10, Y14, and N25 in PiTX-Kα, rather than a change in conformation in this region, can apparently explain the inability of PiTX-Kα to block maxi-K$^+$ channels.

Another important difference between PiTX-Kα and other α-K toxins is that PiTX-Kα has three fewer residues at the N-terminus. In CTX and other α-K toxins, the first three residues form a third β-strand in the antiparallel β-sheet; this strand is absent in PiTX-Kα (Figure 2). Furthermore, removal of the first two residues in CTX by chymotrypsin digestion significantly reduces its affinity (>100-fold) for maxi-K$^+$ channels (Smith, 1988), whereas site-directed mutagenesis of CTX at Phe-2 (F2A, F2W) causes only a 6−13-fold reduction (Goldstein *et al.,* 1994; Stampe *et al.,* 1994). Thus, removing the first two residues in CTX has a more deleterious effect on binding maxi-K$^+$ channels than simply changing the side chain at position 2. Like des-(pyroGlu-1,Phe-2)-CTX, the absence of amino-terminal residues in PiTX-Kα may be an additional reason why PiTX-Kα cannot block maxi-K$^+$ channels.

Why PiTX-Kα Blocks A-Type Channels. As noted above, another goal of these studies was to determine which residues in PiTX-Kα contribute to its high affinity for cloned Kv1.2 channels and A-type channels from rat brain synaptosomes (Rogowski *et al.,* 1996). When the structures of PiTX-Kα and CTX are compared, two regions display backbone and side chain variations that may explain the higher affinity that PiTX-Kα has for A-type channels.

Comparison of CTX and PiTX-Kα structures reveals that no residue in the loop of CTX (residues 22−25) occupies a position in three-dimensional space analogous to Tyr-23 in PiTX-Kα (Figure 5). At position 23, CTX contains a threonine which faces the interior of the protein, whereas PiTX-Kα has a bulky aromatic side chain (Tyr-23) which faces the surface. In addition, PiTX-Kα adopts a different backbone structure from CTX in the loop region between the α-helix and β-sheet. While CTX has no residue equivalent to Tyr-23 in PiTX-Kα, another α-K toxin, AgTX2, does have a large residue (Arg-24) which occupies a similar position. This correlates with the similar affinities
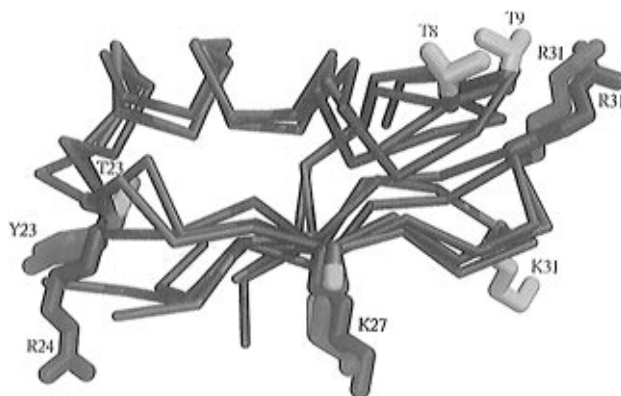

FIGURE 5: Comparison of structures for CTX, PiTX-Kα, and AgTX2 (Krezel *et al.*, 1995) illustrating Lys-27 and residues that confer selectivity for A-type channels. Overlay of α-carbon traces (gray, tinted with yellow for CTX, magenta for PiTX-Kα, or green for AgTX2). Selected side chains for PiTX-Kα (magenta), AgTX2 (green), and CTX (yellow) are shown. Two additional residues for CTX (T8, T9) are included since they are known to interact specifically with residue 425 of the Shaker potassium channel (Goldstein *et al.,* 1994).

that AgTX2 and PiTX-Kα have for A-type channels (Rogowski *et al.*, 1996; Hidalgo & MacKinnon, 1995). AgTX2 selectively blocks A-type K$^+$ channels, and the R24Q mutation in AgTX2 reduces affinity for the Shaker channel 1000-fold (Hidalgo & MacKinnon, 1995). Further analysis of pairwise channel/toxin mutants indicates that, at least for AgTX2, this residue is in contact with Asp-431 of the Shaker F425G channel (Hidalgo & MacKinnon, 1995). The similarities between these two toxins raise the possibility that Tyr-23 of PiTX-Kα forms a hydrogen bond with Asp-431 or another residue nearby on A-type channels.

Another difference between the structures of PiTX-Kα and CTX occurs in the β-turn. PiTX-Kα has an arginine residue at the third position of the turn, whereas CTX has a lysine. Inspection of the three-dimensional structures for these toxins, however, reveals that the side chain of Arg-31 in PiTX-Kα is in a quite different location from that of Lys-31 in CTX (Figure 5; Bontemps *et al.,* 1992). This difference occurs because PiTX-Kα forms a type II turn, while CTX forms a type I turn (Bontemps *et al.,* 1992). As a result of this difference, Arg-31 in PiTX-Kα is located in a region of the toxin that includes residues Thr-8 and Asn-9. Using Miller and co-workers' model for toxin−channel interactions, the analogous residues of CTX (T8, T9) interact with Phe-425 of the Shaker channel (Figure 5; Goldstein *et al.,* 1994). In other studies involving this region of the toxin, mutation of the residue adjacent to Lys-31 in CTX (N30Q) significantly reduces the affinity for Shaker F425G (1600-fold) with smaller effects on maxi-K$^+$ channels (24-fold) (Goldstein *et al.,* 1994; Stampe *et al.*, 1994). Thus, Arg-31 in PiTX-Kα is located in a region of PiTX-Kα that probably interacts with A-type channels whereas, in CTX, no residue occupies this space (Figure 5; Goldstein *et al.,* 1994).

It is noteworthy that Tyr-23 and Arg-31 of PiTX-Kα are on opposite sides of the molecule (i.e., they are 180° apart). These two residues are in positions analogous to residues Arg-24 and Arg-31 of AgTX2. If both of these residues interact with A-type channels, then they must contact different subunits of the tetrameric channel according to the model of Miller and co-workers (Miller, 1995; Hidalgo & MacKinnon, 1995; Krezel *et al.*, 1995). Since CTX does

not have any residues occupying these positions in its three-dimensional structure, Tyr-23 and Arg-31 of PiTX-Kα (or Arg-24 and Arg-31 of AgTX2) may represent additional sites on the toxin that interact with the channel. These additional interactions could explain the particularly high potency that PiTX-Kα and AgTX2 each have for A-type channels when compared to CTX.

Conclusions. The similarities in the structures of PiTX-Kα and the other members of the α-K toxin family once again verify that these toxins share common secondary structural elements and a similar tertiary fold. Thus, variations in side chain properties and positioning must be responsible for their large differences in affinity and specificity for various K$^+$ channels. Residues implicated for binding maxi-K$^+$ channels are located in well-defined regions of secondary structure. We have shown that amino acid variations in these regions have very little effect on the three-dimensional position of side chains in PiTX-Kα. Generally, the identities of the side chains in these positions can be used to predict whether or not a toxin will inhibit maxi-K$^+$-type channels. The amino acid residues must be S10, W14, R25, and M29 as found for CTX and other subfamily 1 members in order to block maxi-K$^+$ channels with high affinity (Stampe *et al.,* 1994; Goldstein *et al.,* 1994). We postulate that PiTX-Kα does not block maxi-K$^+$ channels because three of the four residues at these positions (P10, Y14, and N25) differ from those found in CTX.

In contrast, we identified two regions of PiTX-Kα (the loop and the tight turn) where significant variations in a toxin's side chains are accompanied by variations in its backbone structure. As a consequence, the channel-blocking activities of different toxins are difficult to predict on the basis of differences in sequence alignments in these regions. However, examination of the three-dimensional structure of PiTX-Kα, together with results from previous mutagenesis studies of α-K toxins, allowed us to suggest roles for residues Y23 and R31 in the binding of PiTX-Kα to A-type channels. The location of these residues in regions such as the loop and turn may not be coincidental; it is precisely these regions of the backbone that are most able to accommodate large changes in amino acid sequence without disrupting the stable fold of the toxin. As more toxins in this family are characterized, an emerging picture of the structural determinants required for their activity should enhance our general understanding of the structure and function of K$^+$ channels.

ACKNOWLEDGMENT

SUPPORTING INFORMATION AVAILABLE

A table of resonance assignments and figures showing tabulated NOE correlations, selected NMR spectra, and a Ramachandran plot of the best structure (6 pages). Ordering information is given on any current masthead page.

REFERENCES

Aiyar, J., Withka, J. M., Rizzi, J. P., Singleton, D. H., Andrews, G. C., Lin, W., Boyd, J., Hanson, D. C., Simon, M., Dethlefs, B., Lee, C., Hall, J. E., Gutman, G. A., & Chandy, K. G. (1995) *Neuron 15*, 1169−1181.

Anderson, C. S., MacKinnon, R., Smith, C., & Miller, C. (1988) *J. Gen. Physiol. 91*, 317−333.

Bartschat, D. K., & Blaustein M. P. (1985) *J. Physiol. 361*, 419−440.

Basus, V. J. (1989) *Methods Enzymol. 177,* 132−149.

Bax, A., & Davis, D. G. (1985) *J. Magn. Reson. 65,* 355−360.

Benishin, C. G., Sorensen, R. G., Brown, W. E., Kruger, B. K., & Blaustein, M. P. (1988) *Mol. Pharmacol. 34*, 152−159.

Blaustein, M. P., Rogowski, R. S., Schneider, M. J., & Krueger, B. K. (1991) *Mol. Pharmacol. 40*, 932−942.

Bontemps, F., Roumestand, C., Gilquin, B., Menez, A., & Toma, F. (1991) *Science 254*, 1521−1523.

Bontemps, F., Gilquin, B., Roumestand, C., Menez, A., & Toma, F. (1992) *Biochemistry 31*, 7756−7764.

Brunger, A. T. (1992) *X-PLOR Version 3.1*, Yale University Press, New Haven, CT.

Crest, M., Jacquet, G., Gola, M., Zerrouk, H., Benslimane, A., Rochat, H., Mansuelle, P., & Martin-Eauclaire, M. (1992) *J. Biol. Chem. 267*, 1640−1647.

Dreyer, F. (1990) *Rev. Physiol. Biochem. Pharmacol. 115*, 94−123.

Fernandez, I., Romi, R., Szendeffy, S., Martin-Eauclaire, M. F., Rochat, H., Van Rietschoten, J., Pons, M., & Giralt, E. (1994) *Biochemistry 33*, 14256−14263.

Ferrin, T. E., Huang, C. C., Jarvis, L. E., & Langridge, R. (1988) *J. Mol. Graphics 6,* 13−27.

Garcia, M. L., Garcia-Calvo, M., Hidalgo, P., Lee, A., & MacKinnon, R. (1994) *Biochemistry 33*, 6834−6839.

Garcia-Calvo, M., Leonard, R. J., Novick, J., Stevens, S. P., Schmalhofer, W., Kaczorowski, G. J., & Garcia, M. L. (1993) *J. Biol. Chem. 268,* 18866−18874.

Goldstein, S. A., & Miller, C. (1993) *Biophys. J. 65*, 1613−1619.

Goldstein, S. A., Pheasant, D. J., & Miller, C. (1994) *Neuron 12*, 1377−1388.

Griesinger, C., & Ernst, R. R. (1987) *J. Magn. Reson. 75*, 261.

Griesinger, C., Sørensen, O. W., & Ernst, R. R. (1985) *J. Am. Chem. Soc. 107*, 6394−6396.

Griesinger, C., Sørensen, O. W., & Ernst, R. R. (1987) *J. Magn. Reson. 75*, 474−492.

Griesinger, C., Otting, G., Wüthrich, K., & Ernst, R. R. (1988) *J. Am. Chem. Soc. 110*, 7870.

Hidalgo, P., & MacKinnon, R. (1995) *Science 268*, 307−310.

Howell, M. L., & Blumenthal, K. M. (1989) *J. Biol. Chem. 264,* 15268−15273.

Huang, C. C., Pettersen, E. F., Klein, T. E., Ferrin, T. E., & Langridge, R. (1991) *J. Mol. Graphics 9,* 230−236.

Johnson, B. A., & Sugg, E. E. (1992) *Biochemistry 31*, 8151−8159.

Kadowaki, H., Kadowaki, T., Wondisford, F., & Taylor, S. (1989) *Gene 76*, 161−166.

Kammann, M., Laufs, J., Schell, J., & Gronenborn, B. (1989) *Nucleic Acids Res. 17,* 5404.

Kessler, H., Greisinger, C., Kerssebaum, R., Wagner, K., & Ernst, R. R. (1987) *J. Am. Chem. Soc. 109*, 607−609.

Krezel, A. M., Kasibhatla, C., Hidalgo, P., MacKinnon, R., & Wagner, G. (1995) *Protein Sci. 4*, 1478−1489.

Laskowski, R. A., MacArthur, M. W., Moss, D. S., & Thornton, J. M. (1993) *J. Appl. Crystallogr. 26,* 283−291.

Lebreton, F., Delepierre, M., Ramirez, A. N., Balderas, C., & Possani, D. (1994) *Biochemistry 33*, 11135−11149.

MacKinnon, R. (1991) *Nature 500*, 232−235.

MacKinnon, R., & Miller, C. (1988) *J. Gen. Physiol. 91*, 335−349.

Macura, S., & Ernst, R. R. (1980) *Mol. Phys. 41*, 95.

Martins, J. C., Ahang, W., Tartar, A., Lazdunski, M., & Borremans, F. A. M. (1990) *FEBS Lett. 260*, 249−253.

Miller, C. (1990) *Biochemistry 29*, 5320−5325.

Miller, C. (1995) *Neuron 15*, 5−10.

Miller, C., Moczydlowski, E., Latorre, R., & Phillips, M. (1985) *Nature 313*, 316−318.

Nilges, M., Clore, G. M., & Gronenborn, A. M. (1988) *FEBS Lett. 229*, 317−324.

Park, C. S., & Miller, C. (1992a) *Biochemistry 31*, 7749−7755.

Park, C. S., & Miller, C. (1992b) *Neuron 9,* 307−313.

Park, C. S., Hausdorff, S. F., & Miller, C. (1991) *Proc. Natl. Acad. Sci. U.S.A. 88*, 2046−2050.

Piantini, U., Sørensen, O. W., & Ernst, R. R. (1982) *J. Am. Chem. Soc*. *104*, 6800.

Piotto, M., Saudek, V., & Sklenar, V. (1992) *J. Biomol. NMR 2*, 661−665.

Possani, L. D., Martin, B. M., & Svendensen, I. (1982) *Carlsberg Res. Commun. 47*, 285−289.

Powers, R., Garret, D. S., March, C. J., Frieden, E. A., Gronenborn, A. M., & Clore, G. M. (1993) *Biochemistry 32,* 6744−6762.

Rance, M., Sørensen, O. W., Bodenhausen, G., Wagner, G., Ernst, R. R., & Wüthrich, K. (1983) *Biochem. Biophys. Res. Commun. 117*, 479.

Rogowski, R. S., Krueger, B. K., Collins, J. H., & Blaustein, M. P. (1994) *Proc. Natl. Acad. Sci. U.S.A. 91*, 1475−1479.

Rogowski, R. S., Collins, J. H., O'Neil, T. J., Gustafson, T. A., Werkman, T. A., Rogawski, M. A., Tenenholz, T. C., Weber, D. J., & Blaustein, M. P. (1996*) Mol. Pharmacol. 50*, 1167−1177.

Schneider, M. J., Rogowski, R. S., Krueger, B. K., & Blaustein, M. P. (1989) *FEBS Lett. 250*, 433−436.

Smith, C. D. (1989) Ph.D. Thesis, Brandeis University, Waltham, MA.

Stampe, P., Kolmakova-Partensky, L., & Miller, C. (1994) *Biochemistry 33*, 443−450.

Stocker, M., & Miller, C. (1994) *Proc. Natl. Acad. Sci. U.S.A. 91*, 9509−9513.

Tenenholz, T. C., Rogowski, R. S., Amburgey, J. C., Collins, J. H., Gustafson, T. A., Blaustein, M. P., & Weber, D. J. (1996) *Biophys. J. 70,* A59

Vallette, F., Mege, E., Reiss, A., & Adesnik, M. (1989) *Nucleic Acids Res. 17*, 723−732.

Werkman, T. R., Kawamura, T., Yokoyama, S., Higashida, H., & Rogawski, M. A. (1992) *Neuroscience 50,* 935−946.

Wishart, D. S., Sykes, B. D., & Richards, F. M. (1992) *Biochemistry 31*, 1647−1651.

Wüthrich, K. (1986) *NMR of Proteins and Nucleic Acids,* John Wiley, New York.